Journal of Nuclear Materials 409 (2011) 207–213

Contents lists available at ScienceDirect

Journal of Nuclear Materials

journal homepage: www.elsevier.com/locate/jnucmat

Thermal creep modeling of HT9 steel for fast reactor applications

Ho Jin Ryu [a,*], Yeon Soo Kim [b], A.M. Yacout [b]

[a] Recycled Fuel Development Division, Korea Atomic Energy Research Institute, 150 Deokjin-dong, Yuseong-gu, Daejeon 305-353, Republic of Korea
[b] Nuclear Engineering Division, Argonne National Laboratory, 9700 S. Cass Ave., Argonne, IL 60439, USA

ARTICLE INFO

Article history:
Received 5 February 2008
Accepted 21 December 2010
Available online 29 December 2010

ABSTRACT

The ferritic martensitic steel HT9 is a primary candidate material for the fuel cladding of liquid–metal-cooled fast reactors (LMFRs) owing to its excellent stability under irradiation. Thermal creep of fuel cladding is a potential life-limiting factor in the long-life fuel design of LMFRs. Using the measured data available in the literature, such as creep strain data, stress rupture data, and steady-state creep rate data, a generalized creep correlation was developed. The new correlation is based on the Garofalo equation and the modified Monkman–Grant equation, and it shows better agreement with the experimental data than existing correlations that use either the theta projection method or the minimum commitment method, making it more appropriate for use in long-life applications.

1. Introduction

Ferritic martensitic steels (FMS) composed of 9–12% Cr such as HT9 are often used as high temperature structural materials in coal power plants and gas power plants. FMS have a higher thermal conductivity and a lower void swelling under irradiation than austenitic stainless steels [1,2]. Thus, HT9 is a primary candidate material for the fuel cladding material of advanced nuclear reactors such as liquid–metal-cooled fast reactors (LMFRs) owing to its excellent irradiation stability.

The nominal alloy composition of HT9 is given in Table 1. The development history of FMS with 9–12% Cr is listed in Table 2; it shows their rupture strength and maximum use temperature have been improved. Although HT9 belongs to the first generation FMS, which were developed as early as the 1960s, it is still a viable cladding material for LMFRs, small modular fast reactors (SMFRs), and advanced burner reactors (ABRs), mainly because of its proven performance records [3,4].

The creep deformation of the cladding is not a critical performance issue for a typical LMFR fuel design provided with a smeared density of about 75% up to a burnup of about 20% [4]. However, for fuel designs that require a higher burnup, long life (e.g., 15–30 years of fuel life), or higher temperature, creep deformation may be a life-limiting factor. Hence, an improved creep correlation that is applicable to such design conditions is desired.

Although the thermal creep of HT9 has been studied for decades for both nuclear and non-nuclear applications [5–9], inconsistencies still exist in the correlations and the experimental data. In the present study, the test data available for the thermal creep tests of HT9 were assessed. A new generalized correlation, applicable to both typical- and long-life fuel designs, was developed for the performance evaluation of LMFR fuel cladding.

2. Existing correlations for creep strain

There are a few thermal creep correlations of HT9 steel that are available in the literature. The most widely accepted are the correlations developed by Amodeo and Ghoniem [5,6] and by Lewis and Chuang [7].

The correlation by Amodeo and Ghoniem [5] employs the minimum commitment method (MCM) and uses time dependent creep strain curves at 873 K, as reported by Sandvik Steels [7]. The MCM is based on the observation that the 1% strain occurs during either the primary creep regime or at the beginning of the secondary creep regime, and that the 5% strain occurs at the boundary between the secondary and tertiary creep regimes. The correlation by Amodeo and Ghoniem uses the following formulae:

$$\varepsilon_T = [1 - \exp(at^{\alpha})] \times 100, \quad \text{for } 0 < t < 0.9t_5 \tag{1}$$

where

$$a = \ln(1 - \varepsilon_1)/t_1^{\alpha} \tag{2}$$

$$\alpha = \ln[\ln(1 - \varepsilon_2)/\ln(0.99)]/\ln(0.9t_5/t_1) \tag{3}$$

where

$$\varepsilon_2 = 0.01\exp(0.9bt_5^2) \tag{4}$$

$$b = \ln 5/t_5^2 \tag{5}$$

* Corresponding author. Tel.: +82 42 868 8845; fax: +82 42 868 8824.
E-mail address: hjryu@kaeri.re.kr (H.J. Ryu).

0022-3115/$ - see front matter © 2010 Elsevier B.V. All rights reserved.
doi:10.1016/j.jnucmat.2010.12.232

Table 1
Nominal alloy composition of the HT9 ferritic steel [2].

Elements	Fe	Cr	Mo	W	Ni	V	C	Mn	Si	S
wt.%	Bal.	11.5	1.0	0.5	0.5	0.3	0.2	0.55	0.4	<0.02

Table 2
Development history of ferritic martensitic steels with 9–12% Cr.

Generation	Years	100,000-h rupture strengths at 600 °C (MPa)	Alloy type	Maximum use temperature (°C)
0	1940–60	40	T22, T9	520–538
1	1960–70	60	EM12, HCM9M, HT9, HT91	565
2	1970–85	100	HCM12, T91, HCM2S	593
3	1985–95	140	NF616, E911, HCM12A	620
4	Future	180	NF12, SAVE12	650

$$\varepsilon_T = \exp(0.9bt_5^{\alpha}), \quad \text{for } 0.9t_5 < t < t_5 \tag{6}$$

$$\varepsilon_T = \exp(ct^{\gamma}), \quad \text{for } t_5 < t < t_r \tag{7}$$

where

$$c = \ln \varepsilon_r / t_r^{\gamma} \tag{8}$$

with

$$\gamma = \ln(\ln \varepsilon_r / \ln \varepsilon_5) \ln(t_r/t_5) \tag{9}$$

In the above equations, ε_T is the thermal creep strain, ε_1 is the 1% strain, *i.e.*, 0.01, ε_5 is the 5% strain, *i.e.*, 0.05, t is time, t_1 is the time-to-1% strain, t_5 is the time-to-5% strain, t_r is the rupture life, and ε_r is the rupture strain. The strains used in this correlation are also functions of the rupture life (t_r) and temperature (T). The rupture life is a function of the effective stress, σ_{eff}, and temperature. The effective stress for the cladding is given by:

$$\sigma_{eff} = \frac{\sqrt{3}}{2}\sigma_\theta \tag{10}$$

where σ_θ is the hoop stress. Amodeo and Ghoniem obtained the time-to-1% strain, the time-to-5% strain, and the elongation to fracture by deriving a best fit of the data from Sandvik Steels. This used a polynomial function of both temperature and rupture time. The coefficients for the functions in the MCM correlation are available in Ref. [6].

The correlation proposed by Lewis and Chuang [7] uses the theta projection method (TPM) [10]. The TPM method is a numerical method employing the following equations:

$$\varepsilon_T = f(\theta, t) = \theta_1[1 - \exp(-\theta_2 t)] + \theta_3[\exp(\theta_4 t) - 1] \tag{11}$$

where

$$\log \theta_i = a_i + b_i T + c_i \sigma_{eff} + d_i \sigma_{eff} T \tag{12}$$

The term a_i, b_i, c_i *and* d_i are the fitting parameters, t is time in s. and T is temperature in K. For long-life applications, the TPM model is known to have advantages over other models because its equations are more suitable for long-life extrapolation [11].

Lewis and Chuang analyzed three sets of HT9 creep strain curves reported by Sandvik Steels. These curves were measured at 773 K and 363 MPa, 823 K and 227 MPa, and 873 K and 105 MPa, from which the coefficients associated with the θ parameters of the TPM in Eqs. (11) and (12) were obtained. Their results are presented in Table 3. In addition to the dataset from Sandvik Steels, Toloczko et al. [8] reported thermal creep data of HT9 steel

Table 3
Coefficients of the TPM in Eq. (12) for HT9 obtained by Lewis and Chuang [7].

Coefficient	$\log \theta_1$	$\log \theta_2$	$\log \theta_3$	$\log \theta_4$
a_i	32.96	−68.70	−57.83	−27.92
b_i	-3.826×10^{-2}	7.193×10^{-2}	6.081×10^{-2}	2.668×10^{-2}
c_i	-3.633×10^{-2}	6.054×10^{-2}	3.278×10^{-2}	2.692×10^{-2}
d_i	2.790×10^{-5}	-3.772×10^{-5}	-1.725×10^{-5}	-1.790×10^{-5}

at temperatures of 758–873 K. In Fig. 1, we compare the creep strains obtained from the MCM and TPM correlations using experimental data from Sandvik Steels [7]. The TPM correlation provides better predictions at 773, 823 and 873 K compared to the MCM correlation, which yields substantial errors at 773 and 823 K in particular.

However, as shown in Fig. 2, the results from both correlations are inconsistent with the data measured by Toloczko et al. at 823 and 873 K. The discrepancies of the MCM and TPM correlations most likely result from insufficient data in their correlation fittings. Therefore, it is infeasible to extrapolate from these correlations for long-life applications.

3. Creep strain and rupture stress correlations

A new creep correlation was developed in this study to overcome the limitations of the existing creep correlations for HT9 (i.e., MCM and TPM correlations). There are two significant aspects of the new correlation. Firstly, it should be noted that the phenomenological background of the existing correlations is insufficient to describe the creep deformation behavior of HT9 steels. Although the steady-state creep rates can easily be obtained from the literature, using typically available three-stage creep data [9], the existing correlations lack the capability of using this invaluable data. Therefore for the new correlation presented in this study, the creep constitutive equation proposed by Garofalo [12] was chosen as a reference function. This enabled the primary creep strain and the linearly time-dependent steady-state creep rate to be independently obtained. Secondly, any updates to the existing correlations are complicated by the need to use creep strain data that is specific to each test condition. Generally, primary creep strain, steady-state creep rates, and creep rupture time have been reported in the literature. The new correlation can more readily incorporate additional data, when necessary through the use of the Garofalo equation.

3.1. Creep correlation for primary and steady-state regimes

We obtained the primary creep strain and steady-state creep rates by considering data from Toloczko et al. and Chin as well as that from Sandvik Steels. The new correlation for the primary and steady-state creep regimes, ε_{ps}, can be expressed as a function of time, t, by using the Garofalo equation.

$$\varepsilon_{ps} = \varepsilon_p[1 - \exp(-mt)] + \dot{\varepsilon}_s t \tag{13}$$

where ε_p is the primary (transient) creep strain, and m is a material constant, and $\dot{\varepsilon}_s$ is the steady-state creep rate. The primary creep strain increases as both the effective stress and temperature increase, and the steady-state creep rate increases in the same manner. Once ε_p, m, and $\dot{\varepsilon}_s$ are known, the creep strain in the primary creep regime and in the steady-state creep regime can be calculated using Eq. (13). Our method for deriving these variables is described below.

Fig. 3 shows that the primary (transient) creep strains for HT9 are fitted to the reported data by Sandvik Steels [7] and Toloczko

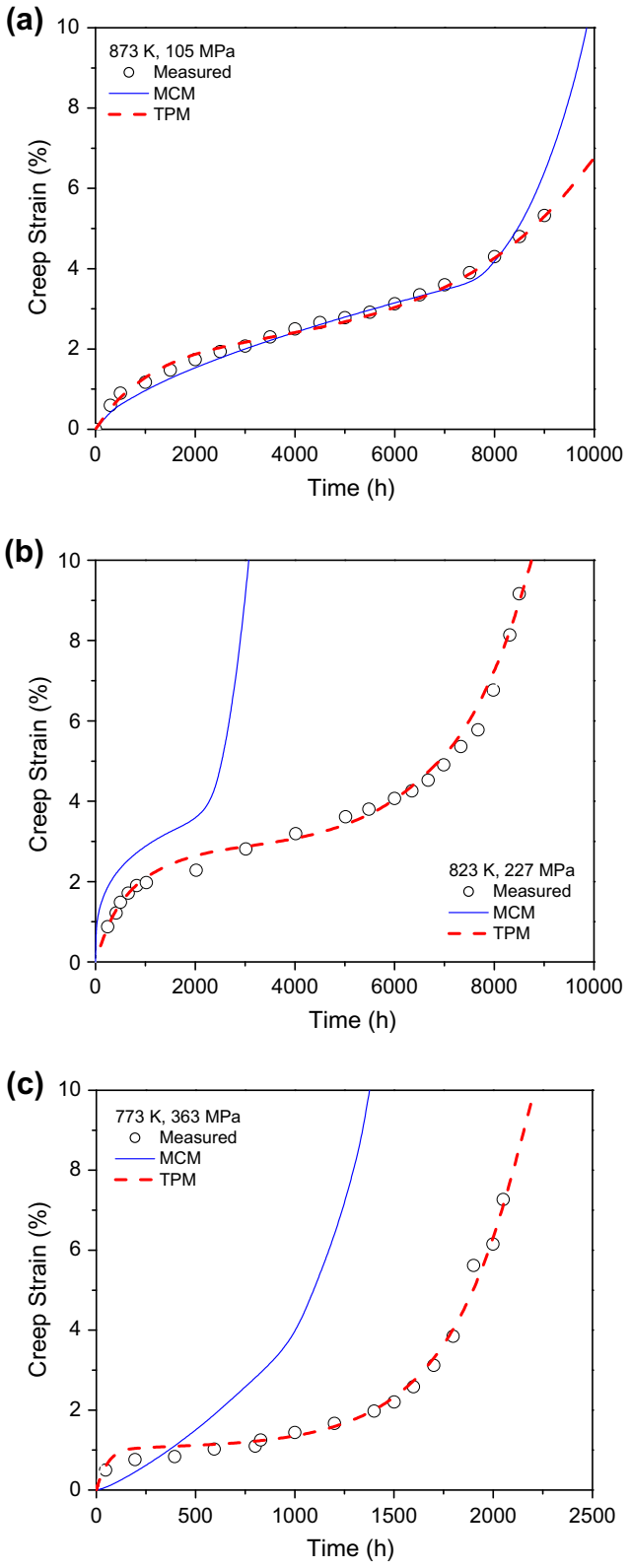

Fig. 1. Comparison of the creep strains predicted by the MCM and TPM correlations with the measured creep data [7]: (a) 873 K and 105 MPa, (b) 823 K and 227 MPa and (c) 773 K and 363 MPa.

et al. [8]. From this, the primary creep strain has been formulated as follows:

$$\log \varepsilon_p(\%) = P_0(T) + P_1(T) \log \sigma_{eff} \ (\text{MPa}) \tag{14}$$

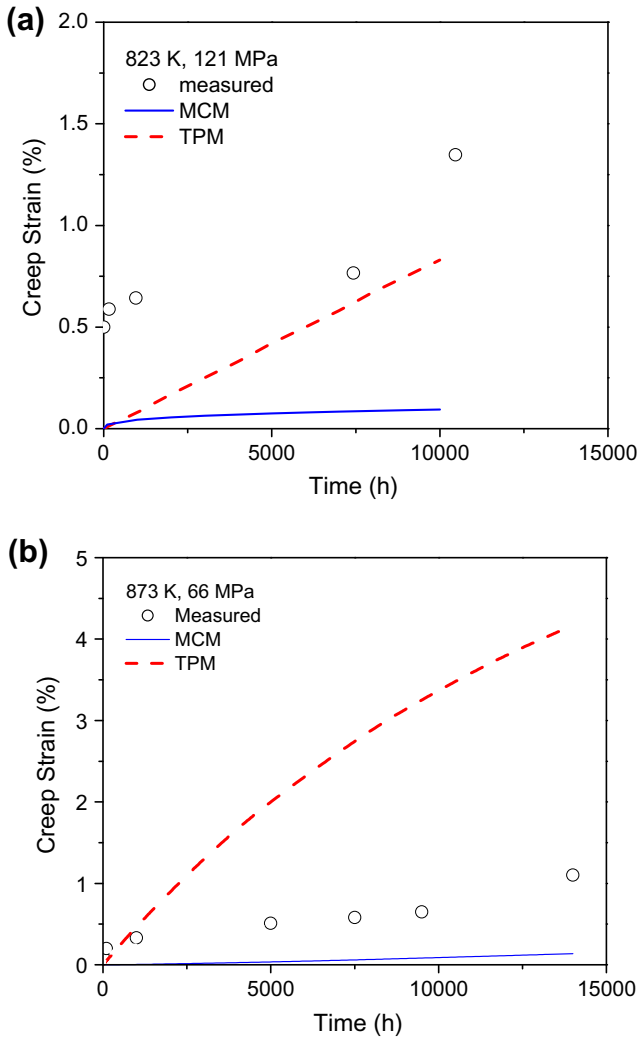

Fig. 2. Comparison of the creep strains predicted by the MCM and TPM correlations and the measured creep strain data [8]. (a) 823 K and 121 MPa, (b) 873 K and 66 MPa.

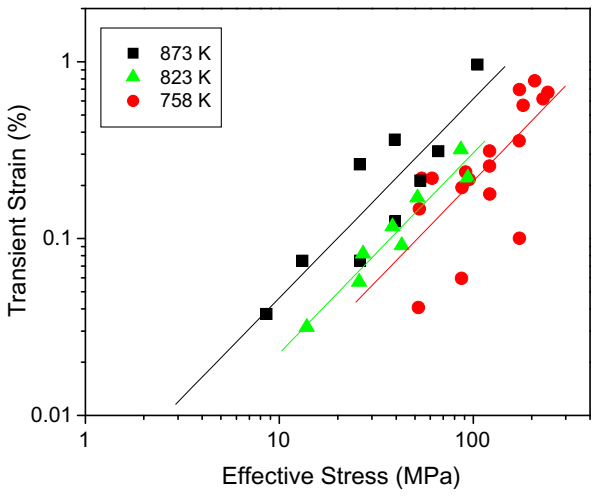

Fig. 3. Primary (transient) creep strains for HT9 fitted to the reported data by Sandvik Steels [7] and Toloczko et al. [8].

where

$$P_0(T) = 0.52 - \frac{2647.31}{T} \quad (15)$$

$$P_1(T) = 1.09 + \frac{31.48}{T} \quad (16)$$

Also, the average value of m in Eq. (13) was found to be 2.11×10^{-6} in s^{-1}.

Chin's [9] report on the steady-state creep rate of HT9 is shown in Fig. 4. The steady-state creep rate shows two distinct stages for the slope (stress exponent) when $\log(\dot{\varepsilon}_s)$ is plotted versus $\log(\sigma_{eff})$. Chin's data exhibit power-law creep behavior which consists of two distinct regimes with different stress exponents. The stress exponent in the power-law creep equation can be obtained from a log–log plot, and it was found to vary from 1.5 to 19.7 with an increase in the effective stress increases. Toloczko et al. [8] explained that the stress exponents in the lower stress exponent regime in Chin's data were indicative of either a diffusion controlled mechanism ($n = 1$) or a dislocation climb–glide mechanism ($n = 2$). The variable stress exponent was also observed in other FMS, such as T91 and P92 [13]. The high stress exponent prevailed when the precipitate density was high, as this hindered dislocation movement. When the initial dislocation density was high, the dislocations tended to tangle themselves and impede their own movement, and vise versa [14].

Data from Toloczko et al. were also used to obtain the steady-state creep rate as shown in Fig. 5. All measured steady-state creep rates form the data from Chin, Toloczko et al., and Sandvik Steels were plotted in Fig. 6. One data point from Sandvik Steel obtained at 873 K and 105 MPa showed good agreement with Chin's data, as shown in Fig. 6. Chin's data yielded higher steady-state creep rates than those obtained from Toloczko's data. Therefore we used Chin's data in the formulation of the new creep correlation so that the predictions of long-term life were conservative.

We formulated a correlation for the steady-state creep strain rate as a function of the effective stress and temperature. Using Chin's data, we obtained the following correlation in the lower stress exponent regime ($n = 1.5$):

$$\log \dot{\varepsilon}_s(s^{-1}) = S_l(T) + 1.5 \log \sigma_{eff}\ (\text{MPa}) \quad (17)$$

$$S_l(T) = -5.58 - \frac{5562.28}{T} \quad (18)$$

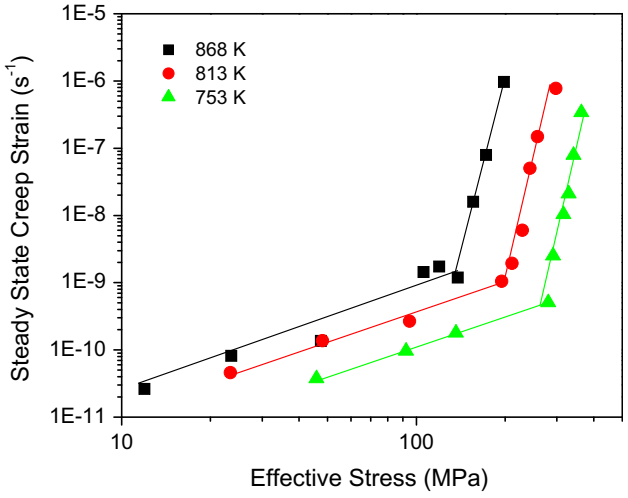

Fig. 4. Steady-state creep strains for HT9 at 753, 813 and 868 K obtained by Chin [9]. Two distinct regimes in terms of the stress exponent are clearly shown.

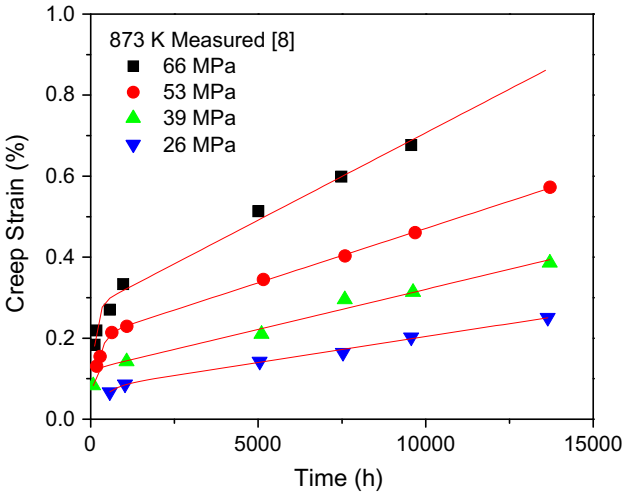

Fig. 5. Creep strain data for HT9 at 873 K reported by Toloczko et al. [8]. The result of curve fitting to the experimental data by the Garofalo equation is shown.

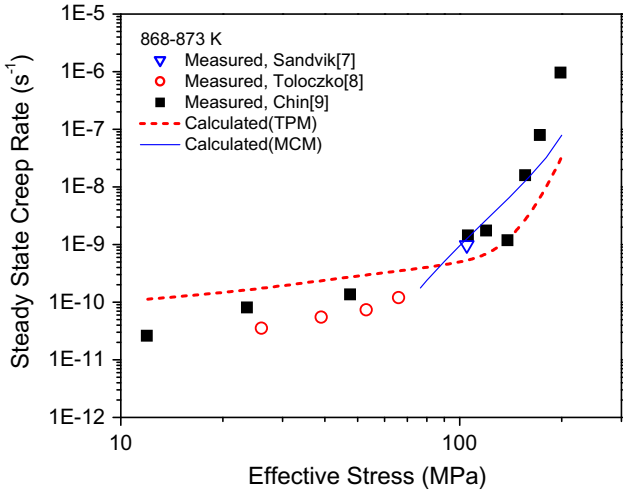

Fig. 6. Steady-state creep rates for HT9 at temperatures of 868–873 K [7–9]. Calculated rates by the TPM method and by the MCM method are added for comparison.

We also obtained the following steady-state creep strain rate in the higher stress exponent regime ($n = 19.7$) as follows:

$$\log \dot{\varepsilon}_s(s^{-1}) = S_h(T) + 19.7 \log \sigma_{eff}\ (\text{MPa}) \quad (19)$$

$$S_h(T) = -13.84 - \frac{32657.11}{T} \quad (20)$$

Therefore, the creep strain in the primary regime and in the steady-state regime can be calculated using Eq. (13) with ε_p and $\dot{\varepsilon}_s$ from Eqs. (14)–(16) and Eqs. (17)–(20), respectively. The expansion of the new creep correlation in the tertiary creep stage is described in Section 3.3.

The time-to-1% strain is considered to be the most critical measurement when evaluating the performance of fuel cladding. Fig. 7 shows the time-to-1% strain predictions at 873 K using the MCM, the TPM and the new correlation. The new correlation predicts that cladding stress should remain below 10 MPa so that the time-to-1% strain is ~30 years at 873 K.

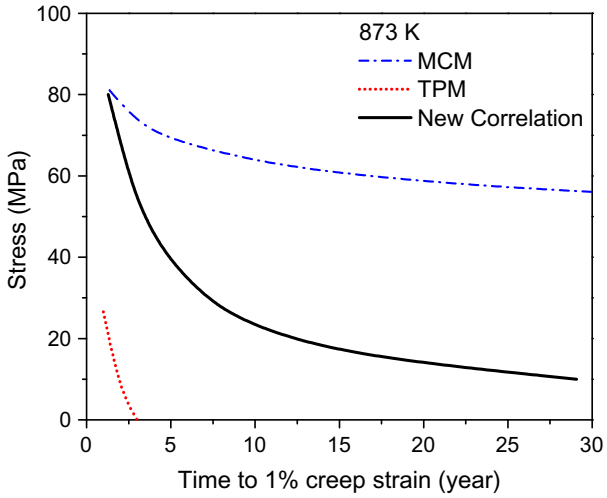

Fig. 7. Comparison of time-to-1% creep strains at 873 K predicted by the MCM method, the TPM method, and the new correlation developed in the present study.

3.2. Creep rupture correlations

Although creep rupture is not directly related to creep strain, creep rupture time can be used to estimate creep strain rates given a few reasonable assumptions. Therefore, the creep rupture data of HT9 were collected from the literature. The creep rupture data in the temperature range of 773–873 K, reported by Sandvik Steels, are shown in Fig. 8 [15]. A least-square linear fit on a log–log scale was used to obtain the coefficients for the new correlation, in which the effective rupture stress can be expressed as a function of the rupture time.

$$\log \sigma_r = R_0(T) + R_1(T) \log t_r \tag{21}$$

where σ_r is the effective rupture stress in MPa, and t_r is the rupture time in h. The coefficients R_0 and R_1 can be written as a function of temperature as follows:

$$R_0(T) = 32.65 - \frac{49039}{T} + \frac{20048000}{T^2} \tag{22}$$

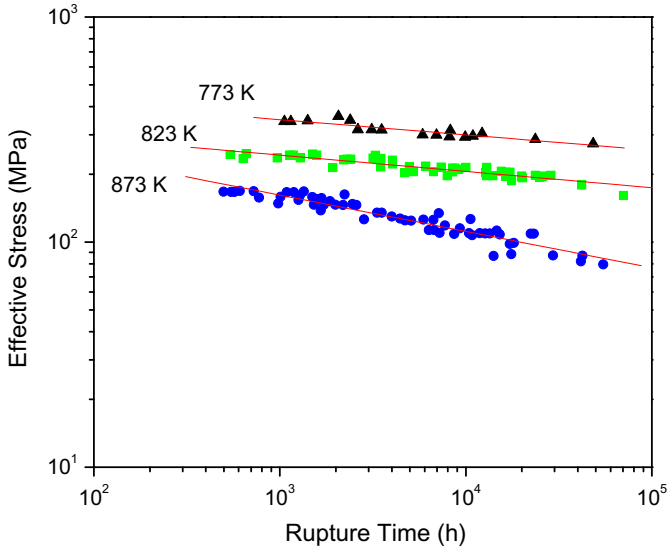

Fig. 8. Stress rupture data for HT9 measured at 773, 823, and 873 K [15].

$$R_1(T) = -12.97 + \frac{20373}{T} - \frac{8041900}{T^2} \tag{23}$$

where T is the temperature in K.

3.3. Creep model for tertiary creep regime

In general, a creep strain correlation can be validated if, at a given rupture time and effective stress, the total creep strain calculated by the correlation equals the measured elongation-to-failure. The rupture time and steady-state creep rate are correlated according to the Monkman–Grant relationship [16]:

$$t_r \dot{\varepsilon}_s^q = C \tag{24}$$

where t_r is the rupture time, $\dot{\varepsilon}_s$ is the steady-state creep rate, and q is a power close to unity. According to Eq. (24), C is the creep strain predicted by the steady-state creep at the point of rupture. A plot showing the separate contributions of primary creep strain, steady-state creep strain and tertiary creep strain to the total creep strain is presented in Fig. 9a. By multiplying the rupture time by the steady-state creep rate of the experimental creep strain data reported by Sandvik Steels [7], we found that C was approximately 4% for HT9 at 823–873 K

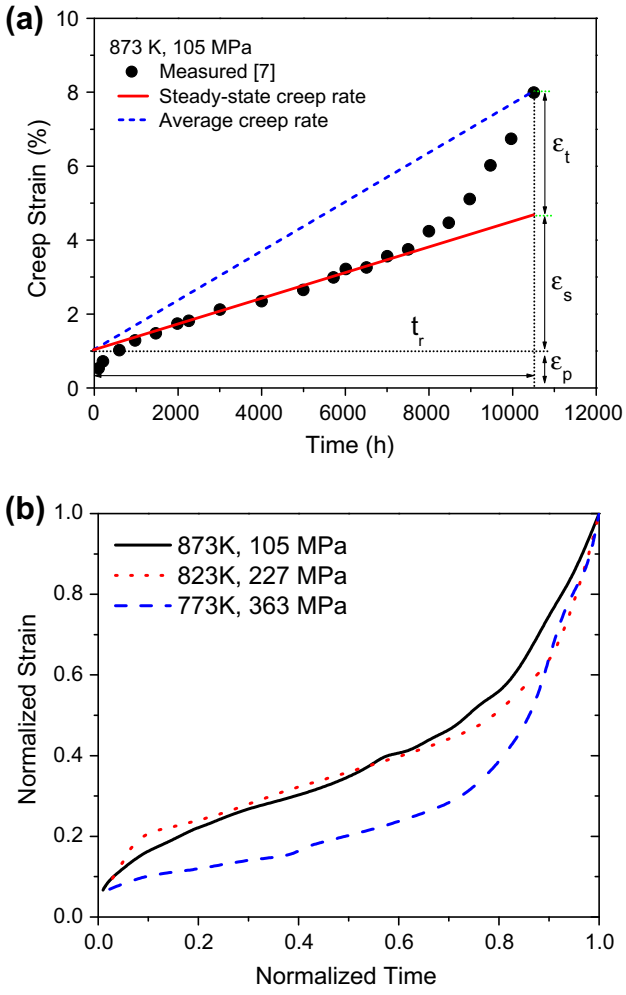

Fig. 9. (a) A plot showing the separate contributions of primary creep strain, steady-state creep strain and tertiary creep strain to the total creep strain. (b) Comparison of normalized strain vs. normalized time plots for three test conditions [7].

Phaniraj et al. [17] proposed a modified Monkman–Grant relationship by introducing the concept of a damage tolerance factor, λ. This was defined as the ratio of the average creep rate to the steady-state creep rate, as follows:

$$\lambda = \varepsilon_r/\varepsilon_s = \dot{\varepsilon}_{ave}/\dot{\varepsilon}_s \tag{25}$$

$$\varepsilon/\varepsilon_r = 1 - (1 - t/t_r)^{1/\lambda} \tag{26}$$

Eq. (26) give the total creep strain once λ, ε_r and t_r are known. Using Eq. (25) to analyze the experimental creep strain curves for 823–873 K, the value of λ was computed to be approximately 2.2. However, as shown in Fig. 9b, λ is not actually a constant. Normalized creep curves for 873, 823, and 773 K indicate that λ is greater than 2.2 at 773 K. Therefore, additional creep strain curves are required to compute λ correctly as a function of temperature and stress.

When a 4% steady-state creep strain at the time of rupture is assumed, for temperatures of 823–873 K, the new correlation predicts a stress versus rupture time which is consistent with the measured data. This is shown in Fig. 10a. The MCM and TPM methods using a 10% total strain at the rupture time are also plotted in Fig. 10a, assuming a typical elongation-to-failure of 5–10% for FMS with 9–12% Cr [18]. The MCM method yields similar results compared to the new correlation, although the TPM method shows a large discrepancy after 10,000 h. Furthermore, the 100,000-h creep stress at 873 K estimated by the TPM method is about 30 MPa, which is much smaller than the reported value of approximately 65 MPa in Ref. [15]. Note that an approximate steady-state creep rate can be obtained by dividing the 4% steady-state creep strain with the creep rupture time. This approach shows a very good agreement with the measured data as shown in Fig. 10b.

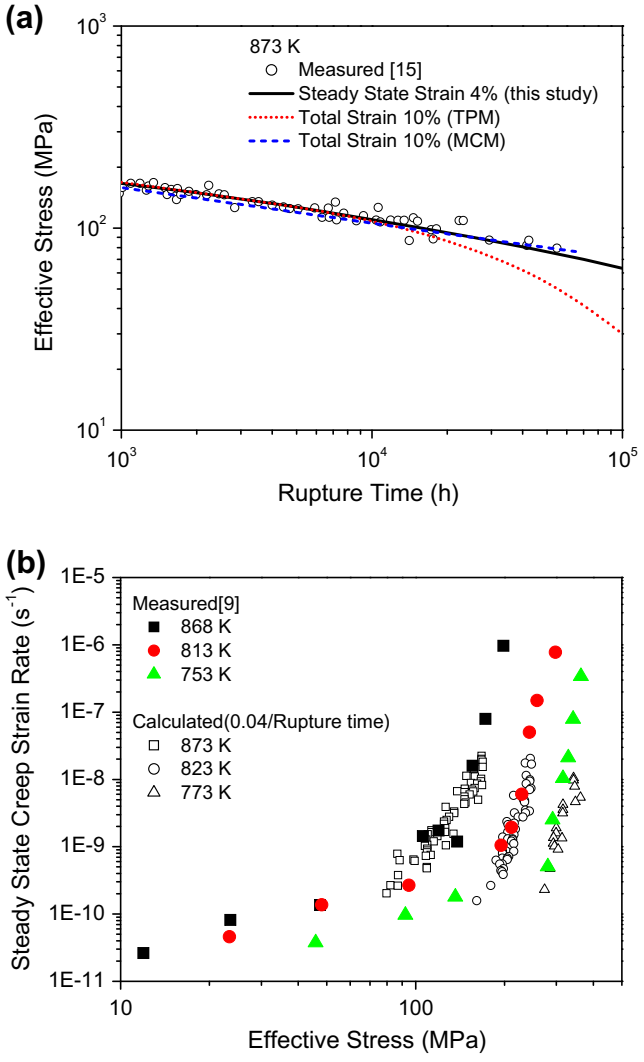

Fig. 10. (a) Comparison of stress vs. rupture time between the measured data and prediction by the new correlation for the 4% steady-state creep strain. The predictions by the TPM and MCM methods for stress-to-10% strain vs. time-to-10% strain are added for comparison. (b) Comparison of steady-state creep rate between the measured data and the prediction by the new correlation dividing the 4% steady-state creep strain with the rupture time.

4. Discussion

Thus far, our paper has focused on HT9 thermal creep correlations. However, since nuclear fuel cladding is commonly used in high energy neutron irradiation environments, it is important to consider the effect of irradiation. Irradiation displaces atoms from their equilibrium position to form vacancies and interstitials. These form voids and dislocation loops, thereby affecting creep deformation. The question arises as to what extent the irradiation enhancement influences the thermal creep. Toloczko et al. [8,19] showed that at low temperatures (below 823 K) the irradiation creep is indeed more significant than the thermal creep. However, at 823 K or higher (typical operating condition for fast reactor cladding) their results showed that the irradiation creep was negligible, due primarily to the active thermal recovery of defects. It is therefore reasonable to just consider the thermal creep at temperatures above 823 K.

The data used in formulating the correlations for each creep regime are shown in Table 4.

For the primary creep regime, we used data from Toloczko et al. and Sandvik Steels. Note that Chin does not present data for the primary creep regime. For the steady-state creep regime, we combined data from Chin, Toloczko et al., and Sandvik Steels. Chin's data was mainly used to provide a conservative steady-state creep model. Rupture data from Sandvik Steels was used for creep rupture modeling. In all applications, the highest quality data amongst that which was available was used.

Since the tertiary creep of HT9 steels starts after 5% strain, the time-to-1% strain results depend only on the primary creep and the steady-state creep regimes. The time-to-1% strain is considered to be the most critical measurement for evaluating the performance of fuel cladding. Therefore, for the performance evaluation of fuel cladding, only the primary and secondary creep equations given by Eqs. (13), (14), (17), (19) need to be used.

A comparison of the time-to-1% strain results at 873 K as predicted by the MCM, the TPM, and the new correlation shows substantial differences, as shown in Fig. 7. The time-to-1% strain value estimated by the new correlation lies between values by the MCM method and the TPM method. The new correlation is apparently less conservative than the TPM method in regards to predicting long-term behavior. It is, however, justified because it better predicts the measured data than the TPM method, as shown in Fig. 10a.

Because the time-to-1% strain is a very important design criterion for an LMFR, the capability of an accurate prediction of this value is an important determinant for the value of any correlation. To ensure a strain below 1% at its end of life, in some circumstances a penalty on fuel cladding temperature may need to be applied. On the other hand, if a high cladding temperature is required, the cladding stress may have to be reduced by increasing plenum volume or cladding thickness. Since the longest test time of the existing data is ~6 years, the new correlation was conservatively fitted to extend the applicability of the measured data beyond this range. Although limited data was assumed in

Table 4
Data used for formulating correlations for each creep regime.

Data Source	Primary creep	Steady-state creep	Creep rupture
Sandvik steels [5–7,15]	Creep strain curves	Creep strain curves	Data values
Toloczko et al. [8]	Data values	Creep strain curves	N/A
Chin [9]	N/A	Data values	N/A

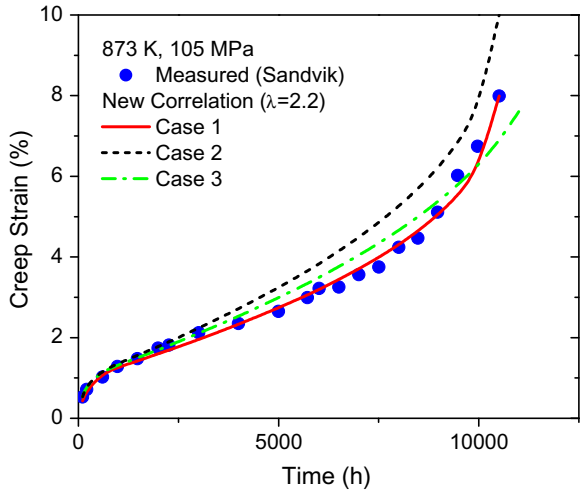

Fig. 11. Prediction of the creep strains for cases 1–3 by the new correlation developed in this study. Case 1 is for known both ε_f and t_f; case 2 is for known t_f from stress rupture data and unknown ε_f; case 3 is for known $\dot{\varepsilon}_s$ and both unknown ε_f and t_f.

its development, the new correlation is nonetheless useful for assessing the long-term (up to ~30 years) thermal creep of HT9 cladding for LMFRs.

By using Eqs. (24)–(26), the total creep strain including the tertiary creep strain can be computed for the following three cases:

- Case 1 with known ε_r and t_r.
- Case 2 with known t_r from stress rupture data and unknown ε_r.
- Case 3 with known $\dot{\varepsilon}_s$ and unknown ε_r and t_r.

Since we have assumed a 4% steady-state strain at the time of rupture, ε_r and t_r can be calculated by using Eq. (26) together with the Monkman–Grant rule, which states that the multiplication between these two unknowns must be 0.04, viz.,

$$t_r\dot{\varepsilon}_s = 0.04 \tag{27}$$

Fig. 11 shows the predicted total creep strains for above three cases using Eqs. (25)–(27) at 873 K and 105 MPa.

The new creep correlation implicitly includes the tertiary creep regime, which was described in Section 3.3, to accommodate the limited availability of necessary data. As can be seen in Fig. 11, the prediction for case 1 is the best fit to the measured data since more data is actually available for this case. Case 3 is a better fit than case 2 in the steady-state regime, which is most likely due to the fact that the steady-state creep rate is well known for case 3. However, the converse in true in the tertiary creep regime, since it is the rupture time instead which is known. For case 2, an overprediction in the steady-state creep regime has occurred.

Unlike stress rupture data, long-life tests for creep strain data are scarce. As shown in Fig. 11, the new correlation's prediction is highly consistent with the measured creep strain up to 1%, despite using incomplete information. This demonstrates the fact that the prediction method developed in this study can be used for long-life applications even when just the stress rupture data are available.

5. Conclusions

The thermal creep strains of HT9 predicted using the correlations available in the literature have been found to be inconsistent. In some cases, they are also inconsistent with the measured data. In this work, a thermal creep correlation based on the Garofalo equation has been developed, and it has been shown to be applicable to both the primary and steady-state creep regimes. For the tertiary creep regime, an implicit model has been proposed by using the modified Monkman–Grant equation. The new correlation has been shown to predict the experimental data better than the correlations available in the literature, particularly for long-term applications.

Acknowledgments

This study was supported in part by Ministry of Education Science and Technology (MEST) of Korea, and in part by the UChicago Argonne, LCC as Operator of Argonne National Laboratory under Contract No. DE-AC-02-06CH11357 between the UChicago Argonne, LLC and the US Department of Energy.

References

[1] R.L. Klueh, Inter. Mater. Rev. 50 (2005) 267.
[2] F. Masuyama, Advanced Heat Resistant Steels for Power Generation, in: R. Viswanathan, J.W. Nutting (Eds.), IOM Communications Ltd., London, 1999 (pp. 33–48).
[3] R.G. Pahl, C.E. Lahm, S.L. Hayes, J. Nucl. Mater. 204 (1993) 141.
[4] G.L. Hofman, L.C. Walters, T.H. Bauer, Prog. Nucl. Energy 31 (1997) 83.
[5] R.J. Amodeo, N.M. Ghoniem, J. Nucl. Mater. 122/123 (1984) 91.
[6] R.J. Amodeo, N.M. Ghoniem, Nucl. Eng. Des. Fusion 2 (1985) 97.
[7] G. Lewis, C.C. Chuang, Fusion Eng. Des. 13 (1991) 407–415.
[8] M.B. Toloczko, B.R. Grambau, F.A. Garner, K. Abe, Effects of Radiation on Materials: 20th International Symposium, ASTM STP1405, West Conshohocken, PA, 2001.
[9] B.A. Chin, Ferritic Steels for use in Nuclear Energy Applications, in: J.W. Davis, D.J. Michel (Eds.), AIME, 1984 (pp. 593–601).
[10] I. LeMay, Principles of Mechanical Metallurgy, Elsevier North Holland, Inc., New York, 1981. p. 367.
[11] R.W. Evans, J.D. Parker, B. Wilshire, Recent Advances in Creep Fracture of Engineering Materials and Structures, Pineridge Press, Swansea, 1982 (pp. 135–142).
[12] F. Garofalo, Fundamentals of Creep and Creep Rupture in Metals, McMillan, New York, 1965.
[13] L. Kolc, V. Sklenicka, A. Dlouhy, K. Jucharova, in: A. Strang, J. Cawley, G.W. Greenwood (Eds.), Microstructural stability of creep resistant alloys for high temperature plant applications, vol. 445–455, IOM, London, 1998.
[14] P.J. Ennis, A. Zielinska-Lipiec, O. Wachter, A. Czyrska-Filemonowiez, Acta Mater. 45 (1997) 4901–4907.
[15] L. Egnell, N.G. Persson, Proc. Int. Conf. Ferritic Steels for Fast Reactor Steam Generators, in: S.F. Pugh, E.A. Little (Eds.), BNES, London, 1978, pp. 212–216.
[16] F.C. Monkman, N.J. Grant, Proc. ASTM 56 (1956) 593.
[17] C. Phaniraj, B.K. Choudhary, K. Bhanu Sankara Rao, Baldev. Raj, Scripta Mater. 48 (2003) 1313.
[18] AFCI Materials Handbook, Design Properties of HT9 and Russian Ferritic/Martensitic Steels, Revision 4, 2003, pp. 76–84 (Chapter 18).
[19] M.B. Toloczko, F.A. Garner, in: 18th International Symposium, ASTM STP 1325, ASTM, West Conshohochek, PA, 1999, pp. 765–779.